Laboratory Investigation on Hydraulic Anisotropy Behavior of Unsaturated Soil

Priono[ab], Harianto Rahardjo[abc*], Kalyani Chatterjea[ad], Eng-Choon Leong[ac]
[a] *Interdisciplinary Graduate School, Nanyang Technological University, Singapore*
[b] *Residues & Resource Reclamation Centre, Nanyang Environment & Water Research Institute, Nanyang Technological University, Singapore*
[c] *School of Civil and Environmental Engineering, Nanyang Technological University, Singapore*
[d] *National Institute of Education, Nanyang Technological University, Singapore*

Address of Authors:

Priono
Research Scholar
Interdisciplinary Graduate School - Residues and Resource Reclamation Centre, Nanyang Environment and Water Research Institute
Nanyang Technological University
Blk S2, #B3a-01, 50 Nanyang Avenue
Singapore 639798
Email: priono001@ntu.edu.sg

Harianto Rahardjo
Professor
School of Civil and Environmental Engineering
Nanyang Technological University
Blk N1, #1B-36, 50 Nanyang Avenue
Singapore 639798
Email: chrahardjo@ntu.edu.sg

Kalyani Chatterjea
Associate Professor
National Institute of Education
Blk NIE3, #3-133, Nanyang Walk,
Singapore 637616
Email: kalyani.c@nie.edu.sg

Eng-Choon Leong
Associate Professor
School of Civil and Environmental Engineering
Nanyang Technological University
Blk N1, #1C-80, 50 Nanyang Avenue
Singapore 639798
Email: cecleong@ntu.edu.sg

Corresponding author:

Professor Harianto Rahardjo, Ph.D.
School of Civil and Environmental Engineering
Nanyang Technological University
Blk N1, #1B-36, 50 Nanyang Avenue
Singapore 639798

Tel: (65) 6790 - 5246
Fax: (65) 6791 – 0676
Email: chrahardjo@ntu.edu.sg
Website:
http://www.cee.ntu.edu.sg/aboutus/FacultyDir/Pages/chrahardjo.aspx

Laboratory Investigation on Hydraulic Anisotropy Behavior of Unsaturated Soil

Priono[ab], Harianto Rahardjo[abc*], Kalyani Chatterjea[ad], Eng-Choon Leong[ac]
[*] Corresponding author. Tel: +65-67905246. Fax: +65-67910676. Email: chrahardjo@ntu.edu.sg.
[a] Interdisciplinary Graduate School, Nanyang Technological University, 50 Nanyang Avenue, Block S2-B3a-01, Singapore 639798.
[b] Residues & Resource Reclamation Centre, Nanyang Environment & Water Research Institute, Nanyang Technological University, 1 CleanTech Loop, Singapore 637141.
[c] School of Civil and Environmental Engineering, Nanyang Technological University, 50 Nanyang Avenue, Block N1-01a-01, Singapore 639798.
[d] National Institute of Education, Nanyang Technological University, 1 Nanyang Walk, Block NIE3-03-133, Singapore 637616.

Abstract:

Hydraulic anisotropy behavior of unsaturated soil has not been fully investigated. Direct laboratory measurement and indirect determination of hydraulic anisotropy under drying condition were carried out on statically compacted specimens having different initial conditions. Direct measurement of permeability was carried out using unsaturated triaxial permeameter whereas indirect determination of permeability was performed through statistical estimation via measured drying soil-water characteristic curve (SWCC). In this research, two orientations, specifically horizontal-layering (HL) and vertical-layering (VL) orientations were prepared for a given specimen from statically compacted homogeneous sand-kaolin. The results from both direct measurement and indirect determination of hydraulic anisotropy were in a good agreement. Hydraulic anisotropy under unsaturated condition was found to be similar with that in saturated condition. Moreover, hydraulic anisotropy was reflected in the ratio of transient time during the direct measurements of HL and VL specimens at high matric suctions. On the other hand in the indirect method, hydraulic anisotropy was reflected in the ratio of equalization time during SWCC tests at matric suctions higher than the air-entry value of the soil.

Key words: unsaturated soil; hydraulic anisotropy; permeability; soil-water characteristic curve; laboratory experiment

Introduction

Hydraulic characteristics of soil are described mainly by its permeability and its soil-water characteristic curve (SWCC). Coefficient of permeability relates flow rate to driving potential, which is primarily due to pressure head gradient, of water in the soil medium (Fredlund et al. 2012). Direct measurement of permeability, especially in unsaturated condition, is tedious, time consuming and requires modified apparatus (Leong and Rahardjo 1997b; Goh et al. 2015). Hence, direct measurement of permeability of unsaturated soil is scarce in the existing literature. In this research, direct measurement of permeability was carried out using modified unsaturated triaxial permeameter as proposed by Goh et al. (2015).

Since direct measurement of permeability has numerous constraints, indirect determination of permeability via SWCC is frequently performed (Fredlund and Rahardjo 1993). The SWCC indicates the variation of water storage capacity within the macropores and the micropores of the soil subjected to variation in matric suctions (Fredlund et al. 2012). Laboratory measurement of SWCC requires shorter duration compared to permeability test and is commonly performed in research on unsaturated soils. This paper will focus on the SWCC obtained from drying process only. In this study, drying SWCC test was performed using modified triaxial SWCC apparatus recommended by Goh et al. (2010).

With reference to hydraulic properties of soil, anisotropy is described as the ratio of water coefficients of permeability on major to minor axis of soil (Basak 1972; Mualem 1986; Chapuis et al. 1989; Bear and Cheng 2010; Priono et al. 2016). The major axis indicates the direction which is parallel to the layering of soil whereas the minor axis indicates the perpendicular direction to the layering. Hydraulic anisotropy of a soil may either equal to one (isotropic), larger or less than one (anisotropic). Hydraulic anisotropy of a soil is found to be larger than one in

most of the cases, except for clays at shallow depths where there are many root and worm holes (Bear and Cheng 2010). Laboratory experiments on pure saturated rock, sand and clay indicated that inherent hydraulic anisotropy has an upper limit of four (Basak 1972; Chapuis et al. 1989). Basak (1972) argued that clay may have different hydraulic anisotropy ratios in different soil structures, specifically flocculated and dispersed structures.

Previous research works such as Mualem (1984), Ursino et al. (2000) and Assoluine and Or (2006) focused on understanding hydraulic anisotropy behavior during unsaturated conditions by proposing conceptual models and subsequently, performed analytical or numerical analyses over wide range of possible scenarios. Mualem (1984) proposed conceptual ‘‘layered cake’’ model of soil consisting of many thin parallel layers having discrete hydraulic properties. A uniform density distribution function was used to represent the saturated permeability function of various layers, whereas a power function relationship was assumed between the permeability and the matric suction in order to observe the hydraulic anisotropy behavior. Ursino et al. (2000) considered three different anisotropic configurations in Miller-similar porous media, i.e. only distribution of pore diameters was anisotropic; only density of the pores was anisotropic; both density and pore-size distribution (PSD) were anisotropic. Numerical simulations were performed on a similar problem as defined by Roth and Hammel [1996], but by considering hydraulic anisotropy caused by the different configurations. Both Mualem (1984) and Ursino et al. (2000) concluded that the hydraulic anisotropy could behave dependently or independently with regards to the saturation conditions depending on the prevailing configurations. Furthermore, Assoluine and Or (2006) extended Mualem (1984)’s ‘‘layered cake’’ model to consider effects of bulk density variations within a particular soil type.

There are lacks of comprehensive laboratory investigation on hydraulic anisotropy behavior during unsaturated conditions. Blonquist et al. (2011) measured sample-scale dielectric (A_{Ka}) and electrical conductivity (A_{σ}) anisotropy using parallel-plate time domain reflectometry (TDR) and electrical conductivity cell. The purpose was to predict theoretical dielectric anisotropy (A_{ε}) which can be used to understand hydraulic anisotropy behavior during unsaturated conditions since according to Friedman and Seaton (1996) and Friedman and Jones (2001), hydraulic anisotropy follows the same trend as electrical anisotropy. Priono et al. (2016) performed laboratory measurement on SWCC of compacted soils having different hydraulic anisotropy values. It was observed that hydraulic anisotropy did not affect SWCC of the soil, but affected equalization time during SWCC test. More comprehensive laboratory investigation on hydraulic anisotropy behavior during unsaturated conditions needs to be carried out. In this study, hydraulic anisotropy during unsaturated conditions are directly measured using unsaturated triaxial permeameter as well as indirectly determined from measured soil-water characteristic curve (SWCC). Direct and indirect laboratory measurements on hydraulic anisotropy during unsaturated conditions are widely-known to have long testing duration, therefore this study focuses on one soil type i.e. statically compacted sand-kaolin mixtures, but having two different initial conditions.

Theory

In order to observe hydraulic anisotropy behavior of unsaturated soil, identical-but-different-layered specimens i.e. horizontal-layering (HL) and vertical-layering (VL) orientations specimens, were tested in this research as recommended by Priono et al. (2016). Figure 1

illustrates that both specimens originated from static compaction on a homogeneous soil and are identical apart from the compaction-induced layering direction.

Hydraulic anisotropy of a soil can be measured directly in modified unsaturated triaxial permeameter or indirectly through estimation of permeability via SWCC. Given a particular soil structure in a saturated soil, there are different arrangements and connectivities of the pore-water in the soil. As a consequence, different saturated coefficients of permeability shall be measured in different orientations of water flow. During the drying process of the soil, the amount of pore-water is reduced and if the soil structure does not undergo significant changes, it is expected that directional-dependence of water flow shall be similar with that observed in the saturated condition although at a slower rate. Moreover, Priono et al. (2016) reported that the drying SWCC is unique and not affected by hydraulic anisotropy. The difference in magnitude of unsaturated coefficients of permeability is expected to be similar to that difference observed in the saturated coefficients of permeability of the specimen with HL and VL orientations due to the anisotropy.

In this research, both unimodal and bimodal SWCC data were observed, therefore two different fitting SWCC equations are used. Fredlund and Xing (1994) equation with $C(\psi) = 1$ as recommended by Leong and Rahardjo (1997a), shown in Equation (1), was used for fitting unimodal SWCC data. For fitting bimodal SWCC data, a recent equation proposed by Satyanaga et al. (2013), as shown in Equation (2), was used.

$$\theta_w = C(\psi)\frac{\theta_s}{\left\{\ln\left[e+\left(\frac{\psi}{a}\right)^n\right]\right\}^m} \quad (1)$$

where: θ_w = calculated volumetric water content; θ_s = saturated volumetric water content; e = base of natural logarithm; ψ = matric suction (kPa); a = fitting parameter corresponding to air-

entry value (AEV) of soil (kPa); n = fitting parameter corresponding to maximum slope or inflection point of SWCC; m = fitting parameter corresponding to curvature of the SWCC slope.

$$\theta_w = \left(1 - \frac{\ln\left(1+\frac{\psi}{\psi_r}\right)}{\ln\left(1+\frac{10^6}{\psi_r}\right)}\right)\left[\begin{array}{l}\theta_r + (\theta_{s1} - \theta_{s2})\left(1 - \mathrm{ERFC}\dfrac{\ln\left(\dfrac{\psi_{a1}-\psi}{\psi_{a1}-\psi_{m1}}\right)}{s_1}\right) \\ +(\theta_{s2} - \theta_r)\left(1 - \mathrm{ERFC}\dfrac{\ln\left(\dfrac{\psi_{a2}-\psi}{\psi_{a2}-\psi_{m2}}\right)}{s_2}\right)\end{array}\right] \quad (2)$$

where: ψ_a = parameter representing the air-entry value (AEV) of soil (kPa); ψ_m = parameter representing the matric suction at the inflection point of SWCC (kPa); s = parameter representing the geometric standard deviation of SWCC; ERFC = complementary error function; Subscripts 1 and 2 represent subcurves 1 and 2, respectively.

In indirect determination method, permeability of soil is estimated from its corresponding SWCC using Fredlund et al. (1994) model as expressed in Equation (3). Fredlund et al. (1994) model adopts the same statistical approach as that of Childs and Collis-George (1950) and Kunze et al. (1968) models which divide SWCC into finite intervals of volumetric water content for predicting unsaturated permeability at the corresponding suction. However, Fredlund et al. (1994) carried out integration with respect to logarithmic matric suction, instead of arithmetic matric suction.

$$k_w = k_s \frac{\sum_{i=j}^{N} \frac{\theta(e^y) - \theta(\psi)}{e^{y_i}} \theta'(e^{y_i})}{\sum_{i=1}^{N} \frac{\theta(e^y) - \theta_s}{e^{y_i}} \theta'(e^{y_i})} \quad (3)$$

where: k_w = estimated water coefficient of permeability for a particular volumetric water content (m/s); k_s = measured saturated water coefficient of permeability (m/s); y = a dummy variable of integration representing logarithm of matric suction; θ' = first derivative of volumetric water content as described in SWCC function; i = a counter from "j" to "N"; j = interval number which increases as the matric suction increases; N = total intervals between matric suction associated with AEV and residual volumetric water content.

Specimen Preparation

A mixture consisting of L2-grade kaolin and 20-30 grade Ottawa sand in a 1:1 ratio by dry mass, termed as 50S50K mixture, was used in the experimental program. A 50S50K mixture was selected because it would provide cohesion for good compaction and a SWCC throughout wide matric suction range. Standard Proctor compaction tests were used to obtain the compaction curve of the 50S50K mixture. The standard compaction tests followed the procedure described in ASTM D698–12e1.

After obtaining the compaction curve, two different specimens, namely Specimens A and B were compacted. Both Specimens A and B had the same dry density i.e. 95% of the maximum dry density; however Specimen A was compacted at dry of optimum (w = 12.1%) and Specimen B was compacted at wet of optimum (w = 17.5%) initial conditions. All specimens were made of 50 mm diameter and 30 mm high cylindrical shape compacted at 1 mm/min static loading rate following the procedure described in Ong (1999). Static compaction was used to ensure even

compaction, homogeneity and reproducibility of specimens used for different tests. A set of hydraulic tests, specifically saturated, unsaturated permeability and SWCC, were carried out on all specimens in this research.

For each type of specimen, there were two orientations, specifically horizontal-layering (HL) and vertical-layering (VL) specimens. Different preparation procedures for HL and VL specimens were adopted as recommended by Priono et al. (2016). For HL specimens, the soil sample was placed in a 50mm diameter mould and then compacted statically. For VL specimen, an initially large sample was firstly compacted in order to enable cutting the sample in the VL orientation for obtaining a VL specimen of the same size as that of the HL specimen. This procedure of VL specimen preparation was recommended by Chapuis and Gill (1989) who indicated that this specimen preparation method is suitable for sample of high-quality (undisturbed). In this research, a large mould of 100mm diameter was used to produce a large block of sample. Subsequently, a rectangular section was cut from the sample and followed by rotating it 90^{o} on its broader face such that the specimen layers were oriented vertically. Finally, the sample was trimmed to the same size, as the HL specimen. The block of sample was trimmed using fabricated rectangular and circular cutters as illustrated in Figure 2. Minimal disturbance was achieved by ensuring the absence of crack in the specimens as shown in Figure 3.

Laboratory Experiments

Index properties tests for the soil mixture consisting of specific gravity, Atterberg limits, grain size distribution and soil classification according to the Unified Soil Classification System (USCS) were performed according to ASTM standards as summarized in Table 1.

In this research, a complete set of hydraulic tests i.e. saturated, unsaturated permeability and drying SWCC was carried out on all HL and VL specimens. Saturated permeability tests of all specimens were performed using a triaxial cell with two back pressure systems. At first, the specimens were saturated by applying incremental back pressure and cell pressure with a net confining pressure ($\sigma_3 - u_w$) of 10 kPa until pore-water pressure parameter, B value ($B = \frac{\Delta u}{\Delta \sigma_3}$ where Δu = pore-water pressure change after the increment of confining pressure (kPa) and $\Delta\sigma_3$ = increment of confining pressure (kPa)), was larger than 0.95 as suggested by Head (1986). The specimens were then allowed to consolidate under an effective confining pressure of 25kPa. Two back pressure systems were then used to cause de-aired distilled water to flow upward through the specimen under specific pressure head differences of 5 and 10 kPa. Two pressure head differences were used in order to ensure consistency of the measured saturated permeability. The experiment was stopped when the flow rate of water was constant over a period of time (Samingan et al. 2003). Saturated water coefficient of permeability was then calculated using Darcy's law as described in Equation (4).

$$k_s = \frac{v}{i} = \frac{Ql}{A\Delta h} \tag{4}$$

where: v = velocity of water flow through specimen (m/s); i= hydraulic gradient; Q = flow rate of water through specimen (m^3/s); l = length of the specimen (m); A = cross-sectional area of specimen (m^2); Δh = pressure head gradient (m).

For unsaturated permeability tests, an unsaturated triaxial permeameter similar to those used in Rahimi and Rahardjo (2016), following modifications proposed by Goh et al. (2015), was used in this research. A schematic diagram of the modified permeameter and the permeameter used in the laboratory are shown in Figures 4 and 5, respectively. The modified permeameter

consists of a triaxial cell, top and bottom pedestals and a pair of high air-entry ceramic disks. The modified permeameter is connected to two digital pressure and volume controllers (DPVCs) for pore-water pressure, a DPVC for cell pressure, pore-air pressure control system, four pressure transducers (measuring cell pressure, pore-water pressure at the top of specimen, pore-water pressure at the bottom of specimen and pore-air pressure), data acquisition system, and a personal computer. The pressure transducers were calibrated prior to the test of each specimen.

Important features in the unsaturated triaxial permeameter are spiral grooves in the water compartments and a protruding air pressure outlet on the modified top and bottom pedestals as shown in Figure 6. Two water pressure outlets were placed at the spiral grooves to apply pore-water pressure into the water compartment and then into the specimen through the ceramic disk. A protruding air pressure outlet was constructed in order to apply pore-air pressure into the specimen through the attached sintered bronze in the modified ceramic disk, as shown in Figure 6. The sintered bronze is very porous, which allows the continuity of air between air pressure line and pore-air pressure in the specimen. The modified ceramic disk provided uniform distribution of water and air pressures to the specimen. Slow-setting epoxy was used to glue the sintered bronze to the modified ceramic disk and also to glue the ceramic disk to the modified pedestal.

There were three sets of unsaturated triaxial permeameter used in this study, specifically one and two sets using 1 bar and 5 bar ceramic disks, respectively. There was a need to have a 1-bar triaxial permeameter (measuring up to 90 kPa of suction) since unsaturated permeability of the specimens, especially VL orientations, at low suctions could be higher than the saturated permeability of 5 bar ceramic disk which could lead to inaccuracy of permeability measurement due to flow impedance. Moreover, a longer duration of test was expected when measuring

unsaturated permeability of the specimens at high suction conditions, hence two 5-bar triaxial permeameters (measuring permeability at 200 and 400 kPa of suction) were used. For all types of unsaturated triaxial permeameter, all readings were taken automatically every 5 minutes and stored in the computer, including volume change of the specimens as reflected by the reading from DPVC of cell pressure.

Procedure of unsaturated permeability tests involves saturation, consolidation, matric suction application and lastly, unsaturated permeability measurement. Prior to the test, the ceramic disks on the pedestals were saturated by using de-aired distilled water with pressure of 200 kPa for 24 hours. After the ceramic disk was saturated, the saturated permeability of top and bottom ceramic disks were measured. A cell pressure of 500 kPa was applied to the disk and the outflow rate of water was measured in order to obtain saturated permeability of the disk using Equation (4). The saturation and consolidation of the specimens were conducted in a similar manner to that performed in the saturated permeability test.

For matric suction application stage, the axis-translation technique proposed by Hilf (1956) was used in order to prevent cavitation of water at high matric suction. Cell and pore-air pressures were kept constant during this stage, while the pore-water pressure was decreased incrementally in order to create the intended matric suction. An equilibrium condition was achieved when the water volume change measured by the DPVC became negligible. On top of graphical observation, a criterion following central difference approximation of the Taylor Series, as shown in Equation (5), was used in order to ensure consistent determination of equalization time. Equalization time was taken as the time when the gradient of water volume change curve became zero for the first time.

$$f'(x_i) = \frac{f(x_{i+1}) - f(x_{i-1})}{2h} + O(h^2) \quad (5)$$

where: f'(x_i) = gradient of permeability curve at particular suction; i = counter; h = step size (50 intervals); O (h^2) = truncation error.

The last stage of unsaturated permeability measurement would then be performed. Similar to the procedure used in the saturated permeability test, an upward flow of water through the specimen was created by controlling a pressure head difference of 10 kPa between the top and bottom of the specimen. The unsaturated permeability test was stopped when a steady-state condition, where there was constant water volume change, was achieved for a period of time. In determining the steady-state condition especially for the unsaturated permeability test at high matric suctions, Equation (6) was defined following Equation (5). The steady-state condition was considered to commence at the time when the gradients of two successive steps in water volume did not change for the first time (close to 0).

$$f'(x_{i+1}) - f'(x_i) \approx 0 \quad (6)$$

The measured unsaturated permeability did not solely represent the permeability of the soil specimen since there were influences of ceramic disks on the top and bottom pedestals. ASTM D7664–10 recommends that if coefficients of saturated permeability of the disks are not at least two orders of magnitude higher than the saturated permeability of the soil specimen, the influence of the disks must be taken into account in order to obtain accurate unsaturated permeability of the soil specimen. Therefore, the specimen had to be considered as a three-layered system with the top and bottom ceramic disks as suggested by Samingan et al. (2003) and illustrated in Figure 7.

In this system, average velocities of all three layers are equal due to the continuity requirement as shown in Equation (7).

$$v_{\text{system}} = v_b = v_{\text{soil}} = v_t \quad (7)$$

where: v is average velocity (m/s); Subscripts system, b, soil and t represent three-layered system, bottom disk, soil specimen and top disk.

Subsequently, Equation (7) can be expanded into Equation (8).

$$v_{\text{system}} = (ki)_{\text{system}} = (ki)_b = (ki)_{\text{soil}} = (ki)_t = (ki)_{\text{system}} = (k\text{h/L})_b = (k\text{h/L})_{\text{soil}} = (k\text{h/L})_t \quad (8)$$

where:

k = coefficient of permeability (m/s); i = hydraulic gradient; h = head loss; L = length (m).

Considering that the total head loss is equal to the summation of head loss in each layer, the ultimate form to determine the unsaturated permeability coefficient of the specimen can be written as shown in Equation (9).

$$k_{soil} = \frac{L_s}{\left(\frac{L_{system}}{k_{system}} - \left(\frac{L_t}{k_t} + \frac{L_b}{k_b}\right)\right)} \quad (9)$$

For drying SWCC tests, two modified triaxial SWCC apparatuses as used in Goh et al. (2010) and Priono et al. (2016) were used to obtain SWCC of all HL and VL specimens. The modified triaxial SWCC, as shown in Figure 8, allowed continuous water and air pressure controls (automated suction-controlled) during closed-system drying SWCC tests. Since the modified triaxial SWCC apparatus was not intended to measure permeability, the top and bottom pedestals were not modified and a 5-bar ceramic disk was used at above bottom pedestal only whereas at below top pedestal, a porous stone was used. Testing procedures and matric suction applied in the SWCC tests using the modified triaxial SWCC apparatus are similar to those used in the unsaturated permeability tests. Equilibrium time during SWCC tests was obtained using Equation (5) and the corresponding volume of water was then used to plot the final SWCC by considering volume change of the specimen.

Results and Discussions

Initial conditions of Specimens A and B tested in this study were obtained from the compaction curve of the sand-kaolin mixture (50S50K) as depicted in Figure 9. The maximum dry density of 1.84 Mg/m^3 is observed at the optimum water content of 14.2%. Basic soil properties for Specimens A and B are listed in Table 2.

Both Specimens A and B have a gap-graded grain-size distribution (GSD) curve as depicted in Figure 10. The GSD curve illustrates that 20-30 Ottawa sand predominantly consists of medium-sized sand whereas L2-grade kaolin mainly consists of silt-sized particles.

Saturated permeability tests of Specimens A and B with HL and VL orientations, respectively, were carried out and the results are shown in Table 3. For each type of specimen, VL orientation had a higher water coefficient of permeability compared to HL specimen, as expected. In addition, Specimen A was observed to have a lower hydraulic anisotropy than Specimen B. At the same dry density, soils compacted at wet of optimum have a dispersed soil structure as illustrated in Fredlund and Rahardjo (1993) which may enhance the hydraulic anisotropy compared to soils compacted at dry of optimum which have a flocculated structure.

For unsaturated permeability measurement, saturated coefficients of permeability of 1-bar and 5-bar ceramic disks were found to be 5.60×10^{-8} and 1.75×10^{-8} m/s, respectively. Figures 11 and 12 indicate permeability functions for Specimens A and B with HL and VL orientations, respectively, obtained from the direct measurements using the unsaturated triaxial permeameter. It was observed that Specimens A and B have bimodal and unimodal permeability functions, respectively. The observation agrees with the bimodal and unimodal of SWCCs of Specimens A and B, respectively, which are presented later. Considering that permeability represents the ease of water flow and water can only flow through available pore-water which is reflected in the

SWCC, it is expected that permeability and SWCC are closely related including their shapes. The matric suction applied in unsaturated permeability test of Specimens A and B were slightly different, especially below 50 kPa, due to consideration of their respective bimodal and unimodal characteristics.

Figures 11 and 12 show a similar trend for the unsaturated condition i.e. for a given specimen, VL orientation gave a higher coefficient of permeability compared to that of HL orientation. Unsaturated coefficients of permeability of Specimens A and B obtained using direct measurement can be seen in Tables 4 and 5, respectively. Observations on both Specimens A and B indicate that the hydraulic anisotropy measured in the unsaturated condition showed similarity with those observed in the saturated condition as reflected in Table 3. Different initial conditions and different shapes of permeability functions observed in Specimens A and B are found to yield similar hydraulic anisotropy in the unsaturated and saturated conditions.

For comparison, estimated coefficients of permeability of Specimens A and B from the corresponding measured SWCC using modified triaxial SWCC and unsaturated triaxial permeameter apparatuses are shown in Tables 6 and 7, respectively. It is observed that the results from the estimation using two different apparatuses support the results observed in the direct measurement i.e. hydraulic anisotropy values are relatively constant throughout application of matric suction and are similar to the value measured during saturated condition for each specimen. The observed constant hydraulic anisotropy in this research is in good agreement with Mualem (1984)'s conceptual "layered cake" model of soil consisting of homogeneous thin layers and Ursino et al. (2000)'s conceptual configuration of Miller-similar porous media having anisotropic density of the pores and isotropic pore-size distribution (PSD). The sand-kaolin specimens were prepared using static compaction method following Ong (1999), as described in

Specimen Preparation. Static compaction method ensures that each HL and VL specimen is homogeneous throughout layers and highly reproducible for different tests. A steady and relatively slow static loading rate (1 mm/min) during compaction performed in this research is most likely to be the reason that the HL and VL specimens have configuration similar to one of the Ursino et al. (2000)'s models i.e. similar PSD and only the number of pores are direction-dependent. Therefore, it is reasonable to observe constant hydraulic anisotropy in the compacted specimens tested in this research.

There are two different typical water volume change curves observed during permeability test of all specimens. Figure 13 shows typical water volume curve observed in saturated condition and unsaturated condition of matric suction up to75 kPa. Figure 13 depicts linearly increasing water volume measured right from the beginning of permeability measurement. This observation happens over a period of time which indicates that the steady-state condition has already been achieved. It implies that there is fine connectivity between pore-water in the specimen so that the rate of water flow directly corresponds to the applied pressure gradient.

Figure 14 shows typical water volume curve observed during permeability measurement from matric suction of 90 kPa onwards. The water volume curve has non-linear trend at the beginning and then becoming linear trend after some period. This non-linear period can be termed as transient condition in order to reach the steady-state condition reflected by the linear period afterwards. For a given type of specimen, HL and VL orientations are observed to have different durations of transient time, which are determined using Equation (6), although the cumulative water volumes during this period are similar. There is a significant difference in the typical magnitude of water volume change observed in Figures 13 and 14 since the magnitude of water volume change reflects the magnitude of unsaturated permeability. As shown in Tables 4 and 5,

the magnitude of unsaturated permeability at matric suction of 90 kPa onwards (reflected by Figure 14) is significantly less (up to five orders of magnitude) than that at matric suction up to 75 kPa (reflected by Figure 13) for a given specimen.

The transient time for Specimens A and B are summarized in Table 8. VL orientation is found to have a shorter transient time compared to HL counterpart for a given specimen, as expected, considering that VL has a higher coefficient of permeability compared to HL in every condition. The ratio of the transient time between HL and VL orientations of Specimens A and B, respectively, are observed to resemble the hydraulic anisotropies measured in Tables 4 and 5, respectively. This observation indicates that in high matric suctions, hydraulic anisotropy of a soil obtained from the measurement in the steady-state condition is also reflected in the ratio of its transient time.

For the indirect determination of permeability, SWCCs of Specimens A and B obtained using the modified triaxial SWCC and the unsaturated triaxial permeameter are shown in Figures 15 and 16, respectively. Similar to the shapes of the permeability functions observed in Figures 11 and 12, Specimen A has a bimodal SWCC whereas Specimen B shows a typical unimodal SWCC. This observation agrees with the previous studies of Li and Zhang (2009) and Satyanaga et al. (2013). Bimodal and unimodal SWCCs are closely related to bimodal and unimodal pore-size distributions (PSDs), respectively. Li and Zhang (2009) showed that for unsaturated compacted specimens having bimodal PSD, there were possible changes in the bimodal PSD during soil saturation and drying process. During soil saturation, the distinct bimodal PSD observed in the unsaturated compacted specimen can become significantly weaker because of the swelling of soil aggregates that results in more intra-aggregate and fewer inter-aggregate pores. During drying process, the soil may shrink and consequently, more intra-aggregate and fewer

inter-aggregate pores can be deduced until essentially, there is only one dominant pore size (unimodal PSD soil structure). In addition, Satyanaga et al. (2013) indicated that soils having bimodal grain-size distribution (GSD) can produce unimodal SWCC, depending on the initial condition (dry density and water content) of the soil.

For a given specimen, SWCCs obtained are comparable regardless of orientations (HL or VL) and apparatuses used (modified triaxial SWCC or unsaturated triaxial permeameter). Fitting SWCC parameters for Specimens A and B are shown in Tables 9 and 10, respectively. In agreement with Priono et al. (2016), SWCC is a scalar variable and is not dependent on the direction of soil layering. The results also confirmed that for a given type of specimen, the SWCC obtained is not affected by the different apparatuses used, such as the modified triaxial SWCC or the unsaturated triaxial permeameter. The SWCCs also imply that compacted specimens obtained using the static compaction are of high quality and are highly reproducible as almost identical SWCCs were obtained using different apparatuses. In order to estimate unsaturated permeability independently from the observed scalar behavior of SWCC, optimum (highest possible R^2) SWCC best-fitting parameters for each orientation of each specimen are calculated for both modified triaxial SWCC and unsaturated triaxial permeameter measurements. Subsequently, each optimum SWCC best-fitting parameter is used to estimate the corresponding unsaturated permeability using Equation (3) for Specimens A and B, as shown in Tables 6 and 7, respectively. As discussed previously, the results from the estimation using two different apparatuses support the results from the direct measurement on the hydraulic anisotropy behavior during unsaturated conditions.

In agreement with Priono et al. (2016), hydraulic anisotropy of each specimen is reflected in the ratio of equalization times during the application of matric suctions higher than the air-entry

value (AEV). Tables 11 and 12 indicate equalization times for HL and VL Specimens A and B, respectively. It is as expected that equalization time of VL specimen is faster than that of the HL specimen considering that VL specimen has a higher coefficient of permeability than that of HL specimen. The ratio of equalization time reflects the hydraulic anisotropy regardless the different apparatuses used and the different initial conditions. In addition, a general trend is observed for a given type of orientation and specimen, i.e. equalization time for matric suction application using the unsaturated triaxial permeameter is longer than that measured in SWCC test using the modified triaxial SWCC apparatus. The observation is reasonable since the unsaturated triaxial permeameter has different arrangements compared to the modified triaxial SWCC apparatus, especially on the modified ceramic disk instead of the porous stone used below the top pedestal.

During both unsaturated permeability and drying SWCC tests, small volume change was observed for the specimen. Figure 17 shows typical volumetric strains ($\varepsilon=\Delta V / V_{initial}$) in the specimen observed during the test. The specimen underwent shrinking during the drying test and it is observed that the cumulative volumetric strains for all specimens were less than 5% of its initial volume.

Conclusions

This research finds that hydraulic anisotropy of compacted sand-kaolin measured in the unsaturated condition is similar to that in the saturated condition regardless of the initial compaction conditions. This observation is supported by the results of both direct permeability measurement and indirect permeability determination through the SWCC. In the direct permeability measurement, hydraulic anisotropy is also reflected in the transient time needed to reach the steady-state condition at high matric suctions. In the indirect permeability

determination, hydraulic anisotropy is reflected in the equalization time during SWCC tests at matric suctions higher than air-entry value.

Acknowledgement

The first author would like to acknowledge research scholarship provided by Interdisciplinary Graduate School and Nanyang Environment & Water Research Institute, Nanyang Technological University, Singapore.

References

ASTM D7664-10. 2010. Standard test methods for measurement of hydraulic conductivity of unsaturated soils. *Annual Book of ASTM Standards*, ASTM International, West Conshohocken, PA.

ASTM D2487-11. 2011. Standard practice for classification of soils for engineering purposes (Unified Soil Classification System). *Annual Book of ASTM Standards*, ASTM International, West Conshohocken, PA.

ASTM D422-63e2. 2007. Standard test method for particle-size analysis of soils. *Annual Book of ASTM Standards*, ASTM International, West Conshohocken, PA.

ASTM D4318-10e1. 2010. Standard test methods for liquid limit, plastic limit, and plasticity index of soils. *Annual Book of ASTM Standards*, ASTM International, West Conshohocken, PA.

ASTM D698-12e1. 2012. Standard test methods for laboratory compaction characteristics of soil using standard effort. *Annual Book of ASTM Standards*, ASTM International, West Conshohocken, PA.

ASTM D854-14. 2014. Standard test methods for specific gravity of soil solids by water pycnometer. *Annual Book of ASTM Standards*, ASTM International, West Conshohocken, PA.

Assoluine, S., and Or, D. 2006. Anisotropy factor of saturated and unsaturated soils. *Water Resources Research*, 42, W12403.

Basak, P. 1972. Soil structure and its effects on hydraulic conductivity. *Soil Science*, 114(6): 417-422.

Bear, J. and Cheng, A.H.D. 2010. Modeling Groundwater Flow and Contaminant Transport. New York: Springer.

Blonquist, J.M., Robinson, D.A., Humphries, S.D., and Jones, S.B. 2011. Improved dielectric and electrical conductivity anisotropy measurements using TDR in unsaturated mica. *Vadose Zone Journal*, 10:1097-1104.

Chapuis, R.P and Gill, D.E. 1989. Hydraulic anisotropy of homogeneous soils and rocks: influence of the densification process. *Engineering Geology*, 39:75-86.

Chapuis, R.P., Gill, D.E., and Baass, K. 1989. Laboratory permeability tests on sand: influence of the compaction method on anisotropy. *Canadian Geotechnical Journal*, 26:614-622.

Childs, E.C. and Collis-George, G.N. 1950. The permeability of porous materials. *Proceedings of the Royal Society*, 210A:392–405.

Fredlund, D.G. and Rahardjo, H. 1993. Soil Mechanics for Unsaturated Soils. New York: John Wiley and Sons Inc.

Fredlund, D.G., Rahardjo, H., and Fredlund, M.D. 2012. Unsaturated Soil Mechanics in Engineering Practice. New York: John Wiley and Sons Inc.

Fredlund, D.G. and Xing, A. 1994. Equations for the soil–water characteristic curve. *Canadian Geotechnical Journal*, 31:521–532.

Fredlund, D.G., Xing, A. and Huang, S. 1994. Predicting the permeability function for unsaturated soils using the soil-water characteristic curve. *Canadian Geotechnical Journal*, 31:533-546.

Friedman, S.P., and Jones, S.B. 2001. Measurement and approximate critical path analysis of the pore-scale-induced anisotropy factor of an unsaturated porous medium. *Water Resources Research*, 37:2929–2942.

Friedman, S.P., and Seaton, N.A. 1996. On the transport properties of anisotropic networks of capillaries. *Water Resources Research*, 32:339–347.

Goh, S.G., Rahardjo, H., and Leong, E.C. 2010. Shear strength equations for unsaturated soil under drying and wetting. *Journal of Geotechnical and Geoenvironmental Engineering*, 136(4):594-606.

Head, K.H. 1986. Manual of Soil Laboratory Testing. London: Pentech Press.

Goh, S.G., Rahardjo, H., and Leong, E.C. 2015. Modification of triaxial apparatus for permeability measurement of unsaturated soils. *Soils and Foundations*, 55(1):63-73.

Hilf, J.W. 1956. An investigation of pore-water pressure in compacted cohesive soils. PhD Thesis, U.S. Dep. Of the Interior, Bureau of Reclamation, Design and Construction Div., Denver, CO, 654 pp.

Kunze, R.J., Uehara, G., and Graham, K. 1968. Factors important in the calculation of hydraulic conductivity. *Proceedings - Soil Science Society of America*, 32:760–765.

Leong, E.C. and Rahardjo, H. 1997a. Review of soil–water characteristic curve equations. *Journal of Geotechnical and Geoenvironmental Engineering*, 123 (12):1106–1117.

Leong, E.C. and Rahardjo, H. 1997b. Permeability functions for unsaturated soils. *Journal of Geotechnical and Geoenvironmental Engineering*, 123(12):1118–1126.

Li, X. and Zhang, L.M. 2009. Characterization of dual-structure pore-size distribution of soil. *Canadian Geotechnical Journal*, 46(2):129-141.

Mualem, Y. 1986. Hydraulic conductivity of unsaturated soils: prediction and formulas. Methods of Soil Analysis, Part 1: Physical and Mineralogical Methods. 2nd Edition, Agronomy. American Society of Agronomy, Inc., and Soil Science Society of America, Madison, 799–823.

Mualem, Y. 1984. Anisotropy of unsaturated soils. *Soil Science Society of America Journal*, 48:505-509.

Ong, B.H. 1999. Shear strength and volume change of unsaturated residual soil. MEng Thesis, Nanyang Technological University, Singapore.

Priono, Rahardjo, H., Chatterjea, K., Leong, E.C., and Wang, J.Y. 2016. Effect of hydraulic anisotropy on soil-water characteristic curve. *Soils and Foundations*, 56(2):228-239.

Rahardjo, H., Satyanaga, A., and Leong, E.C. 2012. Effects of flux boundary conditions on pore-water pressure distribution in slope. *Journal of Engineering Geology*, Special Issue on Unsaturated Soils: Theory and Applications.

Rahimi, A. and Rahardjo, H. 2016. New approach to improve soil-water characteristic curve to reduce variation in estimation of unsaturated permeability function. *Canadian Geotechnical Journal*, 53(4):717-725.

Roth, K. and Hammel, K. 1996. Transport of conservative chemical through an unsaturated two-dimensional Miller-similar medium with steady state flow, *Water Resources Research*, 32(6):1653-1663.

Samingan, A.S., Leong, E.C., Rahardjo, H. 2003. A flexible wall permeameter for measurements of water and air coefficients of permeability of residual soils. *Canadian Geotechnical Journal*, 40(3): 559-574.

Satyanaga, A., Rahardjo, H., Leong, E.C., and Wang, J.Y. 2013. Water characteristic curve of soil with bimodal grain-size distribution. *Computers and Geotechnics*, 48:51–61.

Ursino, N., Roth, K., Gimmi, T., and Fluhner, H. 2000. Upscaling of anisotropy in unsaturated Miller-similar porous media. *Water Resources Research*, 36(2):421-430.

List of Tables

List of Figures

Table 1. Index properties testing standards

Index Properties Test	ASTM
Specific gravity	D854-14
Grain-size distribution	D422-63e2
Atterberg limits	D4318-10e1
Soil classification (Unified Soil Classification System)	D2487-11

Table 2. Index properties of the specimens

Basic Soil Properties	Specimen A	Specimen B
Dry density (Mg/m^3)	1.75	
Void ratio, e	0.48	
Water content (%)	12.1	17.5
Saturated water content, w_{sat} (%)	23.7	26.1
Specific gravity, G_s	2.59	
Percent sand (%)	50.0	
Percent silt (%)	37.5	
Percent clay (%)	12.5	
Liquid limit, *LL* (%)	46.7	
Plastic limit, *PL* (%)	27.4	
Plasticity index, *PI* (%)	19.3	
Unified Soil Classification System (USCS)	SM-ML	

Table 3. Saturated coefficients of permeability for all specimens

Types of Specimen	$k_{s,HL}$ (m/s)	$k_{s,VL}$ (m/s)	Hydraulic Anisotropy
A	1.67E-08	5.34E-08	3.20
B	1.92E-09	1.12 E-08	5.83

Table 4. Unsaturated coefficients of permeability of Specimen A obtained using direct measurement

Matric Suction (kPa)	$k_{w, HL}$ (m/s)	$k_{w, VL}$ (m/s)	Hydraulic Anisotropy
5	1.56E-08	4.86E-08	3.12
10	1.20E-08	3.69E-08	3.08
20	1.58E-09	6.23E-09	3.94
30	1.50E-09	5.46E-09	3.64
40	1.19E-09	4.15E-09	3.49
50	8.70E-10	2.85E-09	3.28
75	1.91E-10	5.97E-10	3.13
90	1.27E-10	4.13E-10	3.25
200	2.46E-12	8.50E-12	3.46
400	1.74E-13	5.61E-13	3.22
		Average	3.36

Table 5. Unsaturated coefficients of permeability of Specimen B obtained using direct measurement

Matric Suction (kPa)	$k_{w, HL}$ (m/s)	$k_{w, VL}$ (m/s)	Hydraulic Anisotropy
5	1.82E-09	1.06E-08	5.82
20	1.46E-09	7.98E-09	5.47
35	1.42E-09	7.23E-09	5.09
50	4.23E-10	2.59E-09	6.12
75	8.32E-11	4.81E-10	5.78
90	2.74E-11	1.56E-10	5.69
200	9.93E-13	5.93E-12	5.97
400	1.80E-13	1.07E-12	5.94
		Average	5.74

Table 6. Unsaturated coefficients of permeability of Specimen A estimated from measured SWCC using two different apparatuses

Matric Suction (kPa)	Modified Triaxial SWCC			Unsaturated Triaxial Permeameter		
	$k_{w, HL}$ (m/s)	$k_{w, VL}$ (m/s)	Hydraulic Anisotropy	$k_{w, HL}$ (m/s)	$k_{w, VL}$ (m/s)	Hydraulic Anisotropy
5	1.67E-08	5.34E-08	3.20	1.67E-08	5.34E-08	3.20
10	1.28E-08	4.12E-08	3.22	1.43E-08	4.28E-08	2.99
20	1.10E-09	3.28E-09	2.97	1.48E-09	4.28E-09	2.89
30	1.08E-09	3.24E-09	2.99	1.29E-09	3.67E-09	2.84
40	7.32E-10	2.27E-09	3.10	9.40E-10	2.63E-09	2.80
50	4.20E-10	1.37E-09	3.25	5.03E-10	1.43E-09	2.84
75	1.05E-10	3.61E-10	3.44	1.04E-10	3.01E-10	2.89
90	4.81E-11	1.69E-10	3.51	4.68E-11	1.34E-10	2.86
200	2.35E-12	8.18E-12	3.48	2.95E-12	8.03E-12	2.72
400	1.18E-13	3.79E-13	3.22	1.97E-13	5.50E-13	2.79
		Average	3.24		Average	2.88

Table 7. Unsaturated coefficients of permeability of Specimen B estimated from measured SWCC using two different apparatuses

Matric Suction (kPa)	Modified Triaxial SWCC			Unsaturated Triaxial Permeameter		
	$k_{w, HL}$ (m/s)	$k_{w, VL}$ (m/s)	Hydraulic Anisotropy	$k_{w, HL}$ (m/s)	$k_{w, VL}$ (m/s)	Hydraulic Anisotropy
5	1.92E-09	1.12E-08	5.83	1.92E-09	1.12E-08	5.83
20	1.89E-09	1.10E-08	5.81	1.87E-09	1.06E-08	5.68
35	1.63E-09	9.26E-09	5.68	1.52E-09	7.98E-09	5.25
50	8.92E-10	4.98E-09	5.59	8.54E-10	4.33E-09	5.06
75	1.34E-10	7.88E-10	5.89	1.73E-10	9.60E-10	5.56
90	4.39E-11	2.64E-10	6.01	6.35E-11	3.69E-10	5.82
200	1.43E-12	8.70E-12	6.07	2.31E-12	1.29E-11	5.61
400	1.29E-13	7.73E-13	6.01	2.09E-13	1.07E-12	5.09
		Average	5.86		Average	5.49

Table 8. Transient time observed in Specimens A and B

Matric Suction (kPa)	Specimen A			Specimen B		
	Transient Time of HL (h)	Transient Time of VL (h)	Ratio	Transient Time of HL (h)	Transient Time of VL (h)	Ratio
90	21.35	6.84	3.12	50.72	8.63	5.88
200	27.17	8.13	3.34	62.33	11.17	5.58
400	41.56	13.08	3.18	91.98	16.15	5.70

Table 9. Fitting SWCC Parameters of Specimen A

Fitting Parameters of Satyanaga et al. (2013)	Triaxial SWCC		Permeameter	
	HL	VL	HL	VL
θ_{s1}	0.364	0.349	0.360	0.364
ψ_{a1} (kPa)	10.338	10.110	10.441	9.998
ψ_{m1} (kPa)	11.048	10.888	11.236	11.357
s_1	0.195	0.438	3.782	4.671
θ_{s2}	0.281	0.268	0.237	0.223
ψ_{a2} (kPa)	27.386	26.831	35.248	34.190
ψ_{m2} (kPa)	72.953	76.128	72.973	70.126
s_2	1.234	1.193	1.618	1.480
ψ_r (kPa)	499.958	499.990	499.990	500.003
θ_r	0.051	0.045	0.009	0.015
R^2 (HL Triaxial)	0.999	0.991	0.974	0.983
R^2 (VL Triaxial)	0.988	1.000	0.984	0.990
R^2 (HL Permeameter)	0.968	0.981	0.999	0.998
R^2 (VL Permeameter)	0.981	0.987	0.998	1.000

Table 10. Fitting SWCC Parameters of Specimen B

Fitting Parameters of Fredlund and Xing (1994)	Triaxial SWCC		Permeameter	
	HL	VL	HL	VL
θ_s	0.386	0.385	0.379	0.389
a (kPa)	44.765	44.560	45.316	45.495
n	5.135	4.879	4.279	3.669
m	0.712	0.726	0.695	0.814
R^2 (HL Triaxial)	1.000	1.000	0.988	0.992
R^2 (VL Triaxial)	1.000	1.000	0.989	0.993
R^2 (HL Permeameter)	0.988	0.989	0.999	0.995
R^2 (VL Permeameter)	0.992	0.992	0.996	0.999

Table 11. Equalization times of Specimen A during matric suction application using modified triaxial SWCC and unsaturated triaxial permeameter apparatuses

Matric Suction (kPa)	Modified Triaxial SWCC			Unsaturated Triaxial Permeameter		
	HL	VL		HL	VL	
	Elapsed Time (h)	Elapsed Time (h)	Ratio	Elapsed Time (h)	Elapsed Time (h)	Ratio
30	32.85	9.95	3.30	36.06	11.01	3.27
40	35.01	11.15	3.14	40.74	13.27	3.07
50	36.82	11.48	3.21	41.94	13.96	3.01
75	42.74	13.28	3.22	46.64	14.14	3.30
90	67.34	21.26	3.17	72.29	22.88	3.16
200	146.82	46.88	3.13	154.86	49.19	3.15
400	583.04	181.55	3.21	602.08	190.08	3.17

Table 12. Equalization times of Specimen B during matric suction application using modified triaxial SWCC and unsaturated triaxial permeameter apparatuses

Matric Suction (kPa)	Modified Triaxial SWCC			Unsaturated Triaxial Permeameter		
	HL	VL		HL	VL	
	Elapsed time (h)	Elapsed time (h)	Ratio	Elapsed time (h)	Elapsed time (h)	Ratio
50	57.68	11.15	5.17	65.52	12.49	5.25
75	80.08	13.66	5.86	86.97	14.57	5.97
90	144.15	24.14	5.97	153.01	26.07	5.87
200	288.41	50.49	5.71	301.16	54.58	5.52
400	1078.44	187.90	5.74	1132.02	194.54	5.82

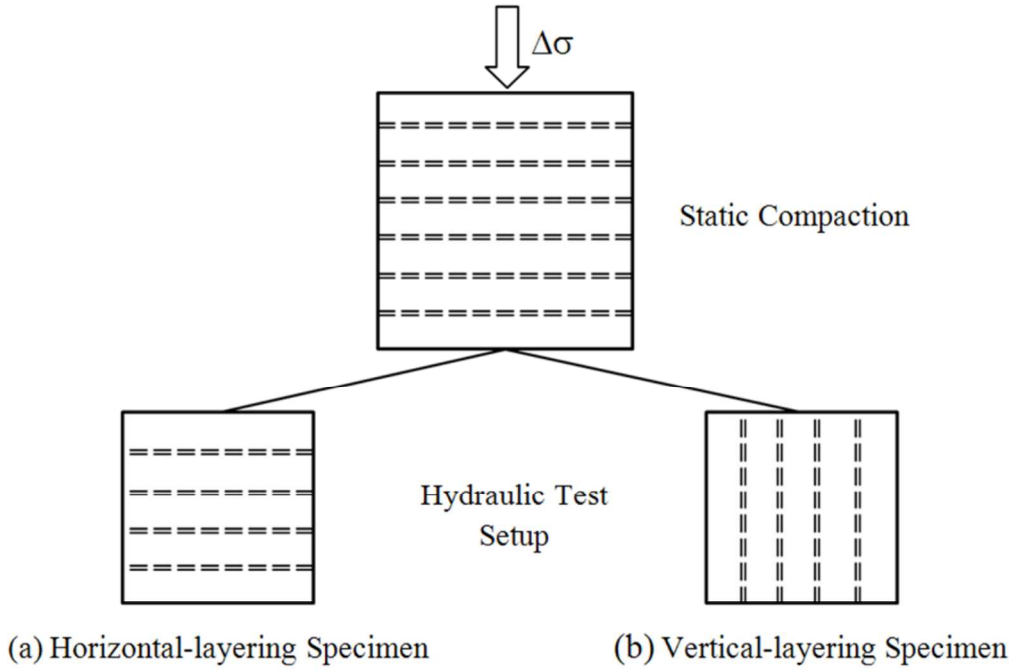

Figure 1. Conceptual sketch of HL and VL orientations of a given specimen from a statically compacted soil mixture

381x285mm (96 x 96 DPI)

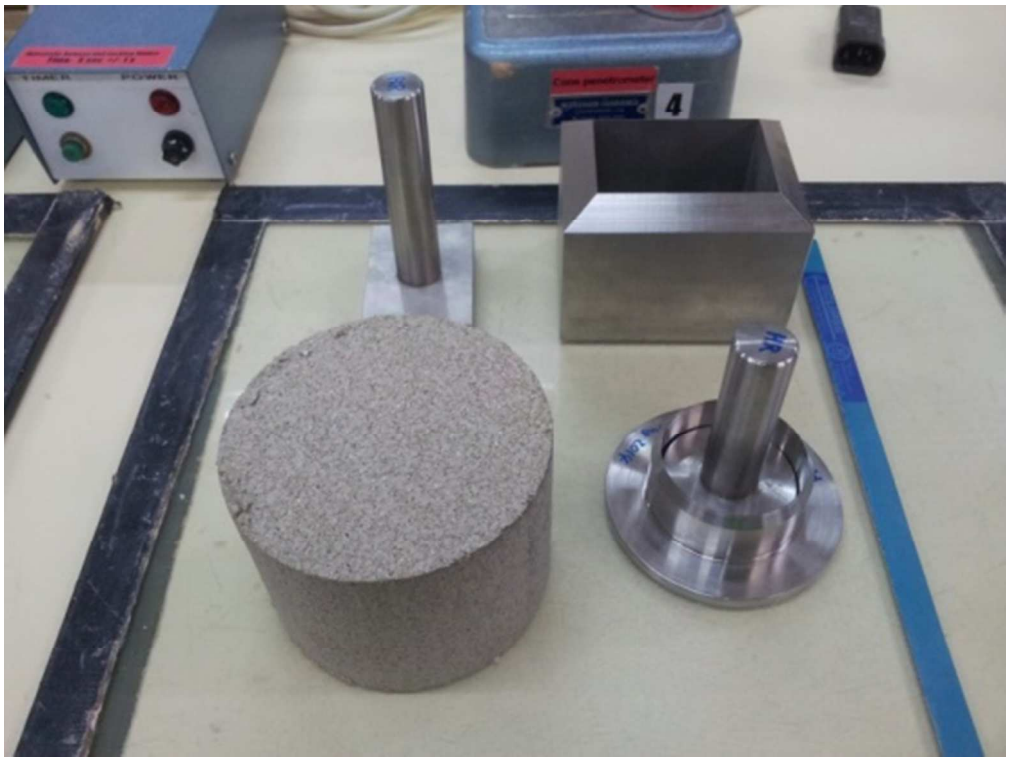

Figure 2. Initial block of sample and cutters used for preparing VL specimens

381x285mm (96 x 96 DPI)

Figure 3. Final VL specimen

381x285mm (96 x 96 DPI)

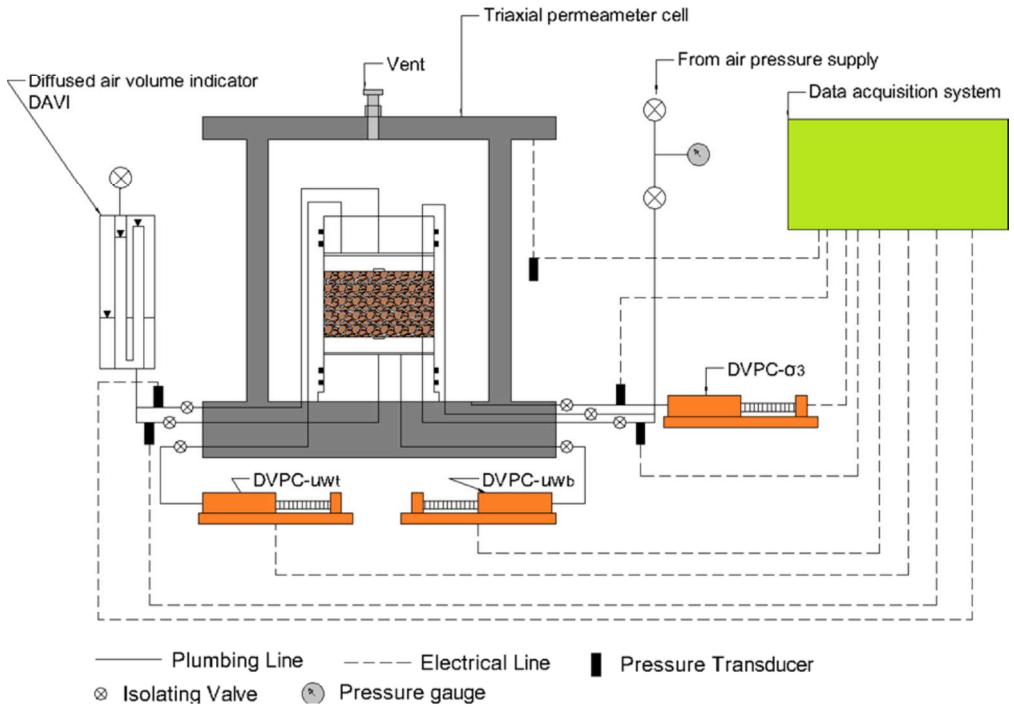

Figure 4. Schematic diagram of unsaturated triaxial permeameter

381x285mm (96 x 96 DPI)

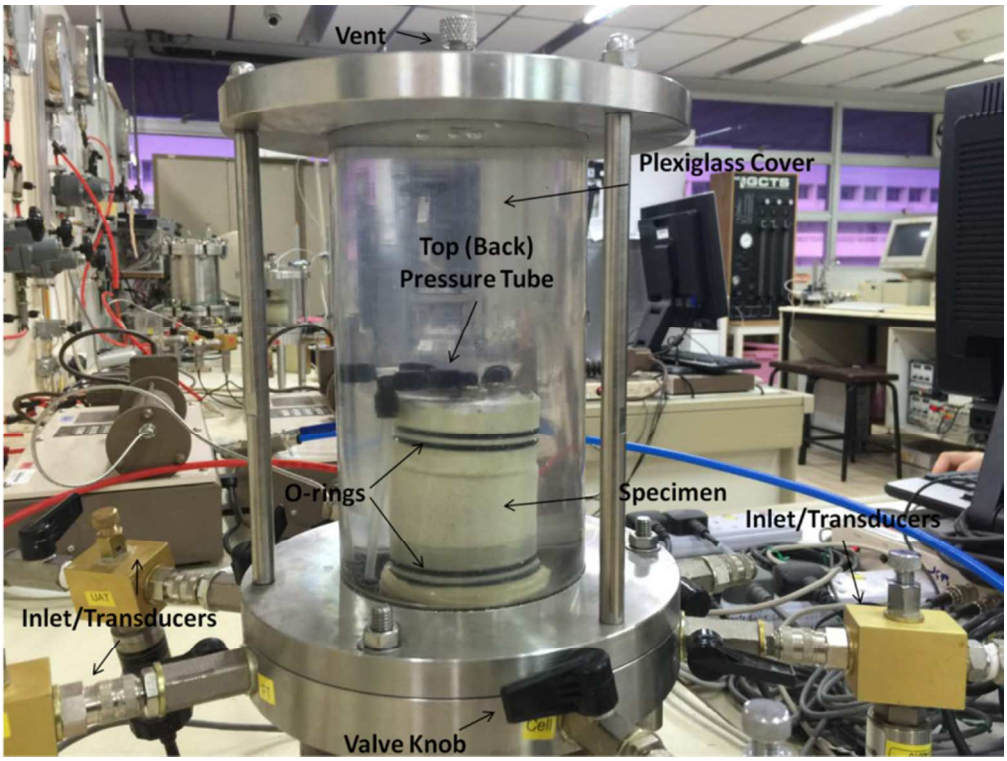

Figure 5. Unsaturated triaxial permeameter in the laboratory

381x285mm (96 x 96 DPI)

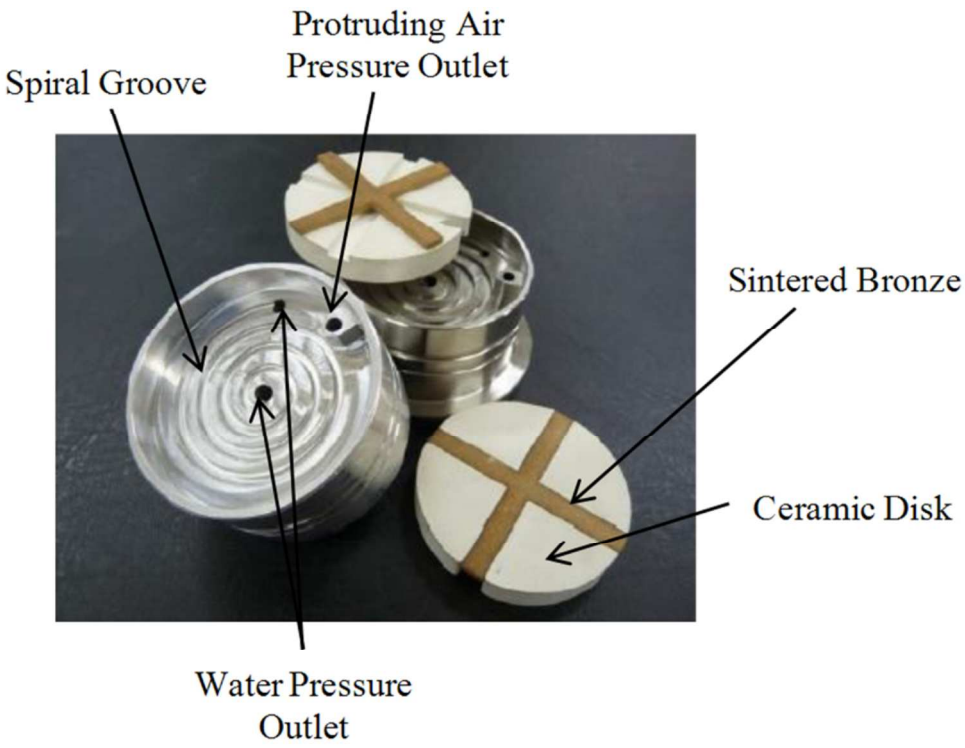

Figure 6. Modified pedestals and modified ceramic disks used in the unsaturated triaxial permeameter

381x285mm (96 x 96 DPI)

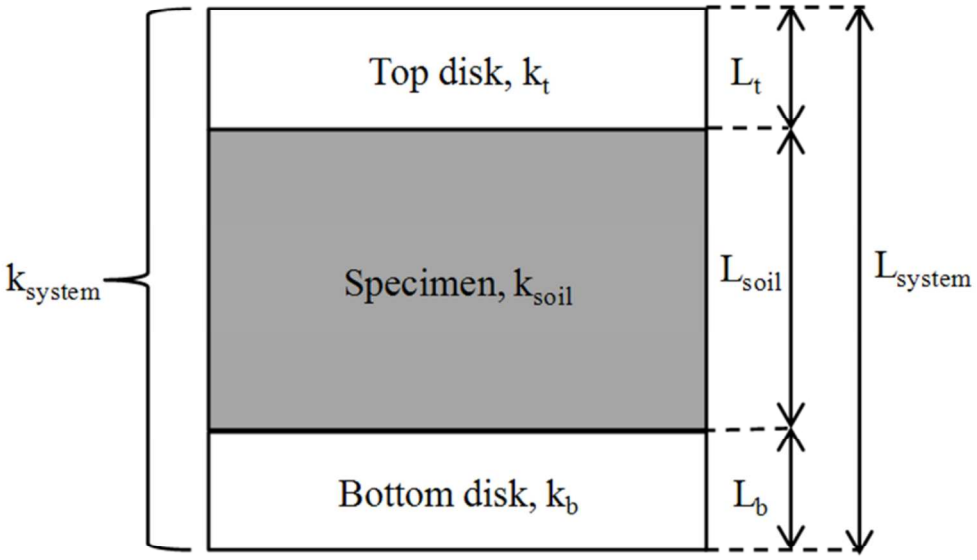

Figure 7. Three-layered system for unsaturated permeability measurement

381x285mm (96 x 96 DPI)

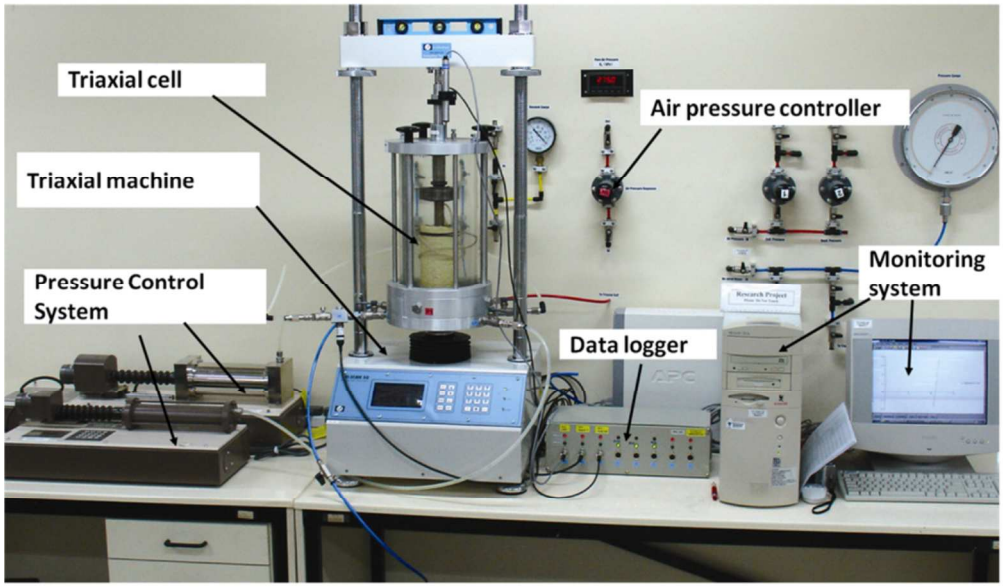

Figure 8. SWCC test performed using modified triaxial SWCC apparatus

381x285mm (96 x 96 DPI)

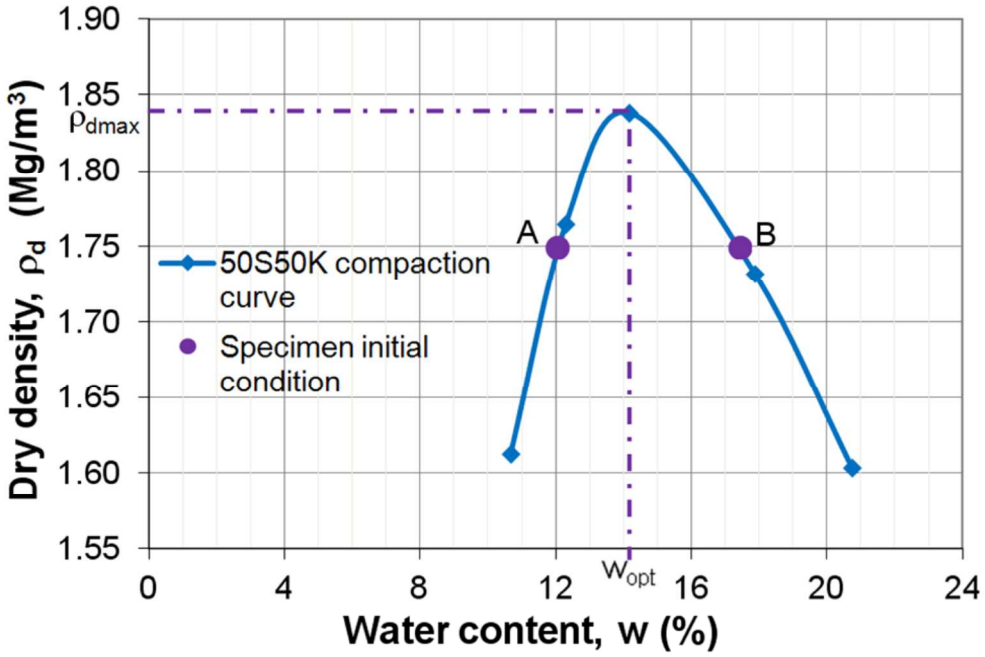

Figure 9. Compaction curve of 50S50K mixture

381x285mm (96 x 96 DPI)

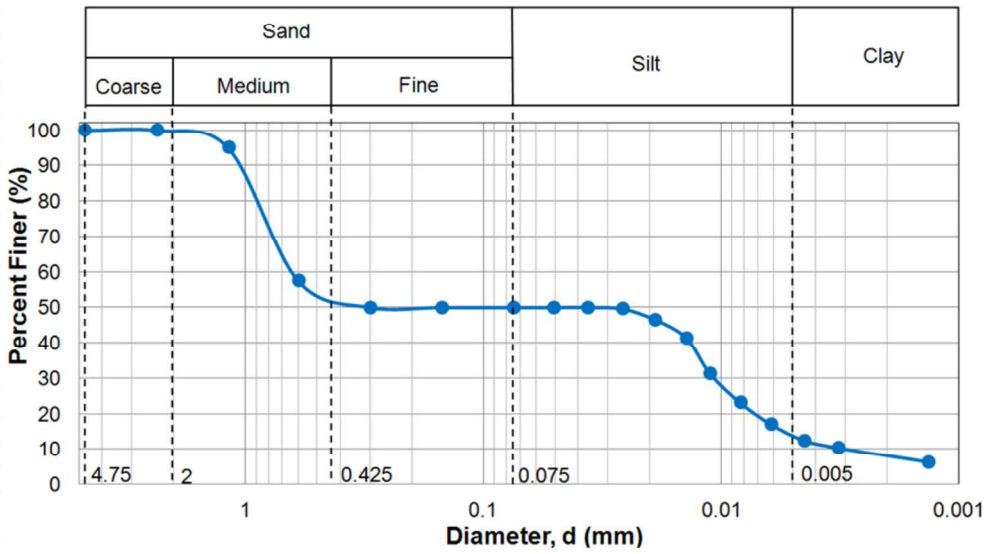

Figure 10. GSD curve of the specimens

381x285mm (96 x 96 DPI)

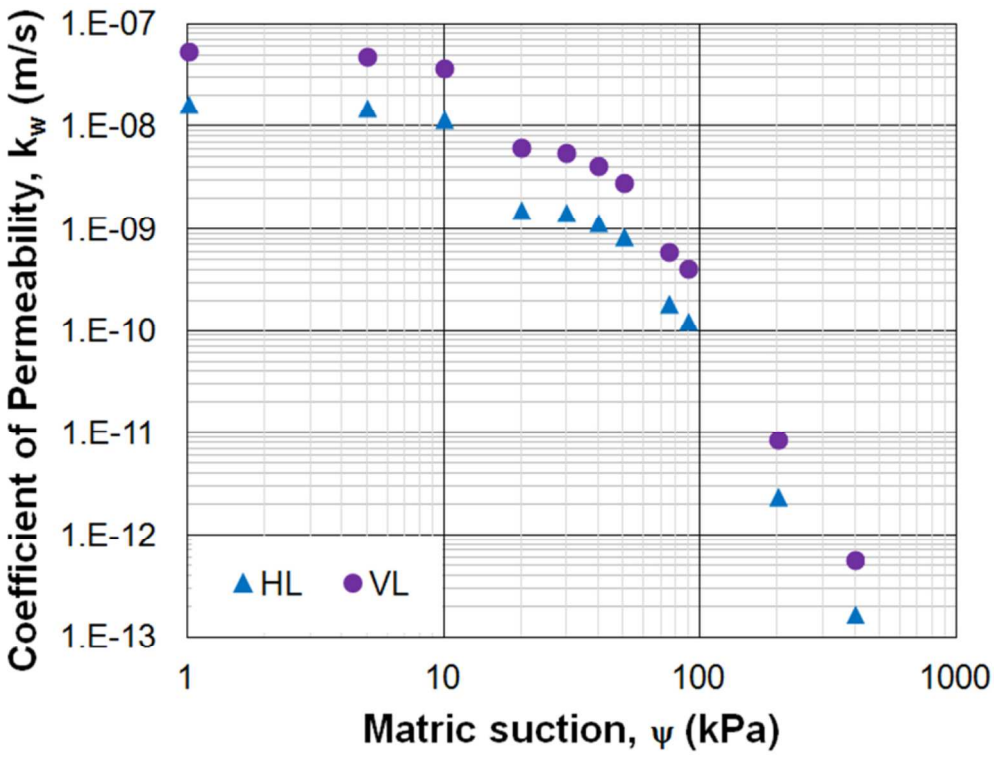

Figures 11. Permeability functions of Specimen A

381x285mm (96 x 96 DPI)

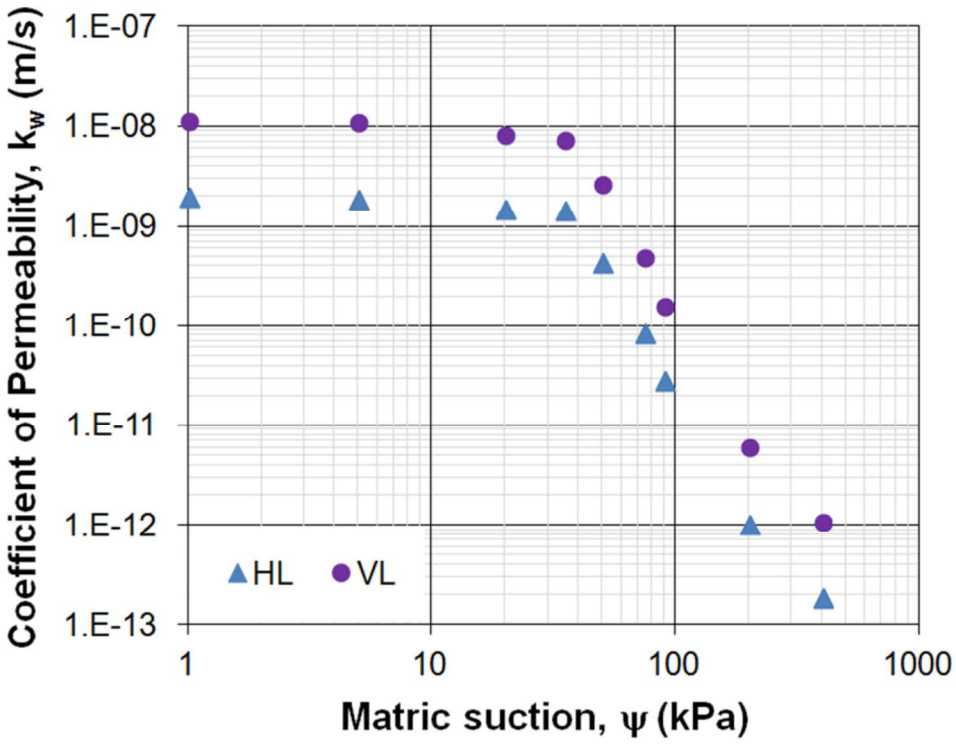

Figures 12. Permeability functions of Specimen B

381x285mm (96 x 96 DPI)

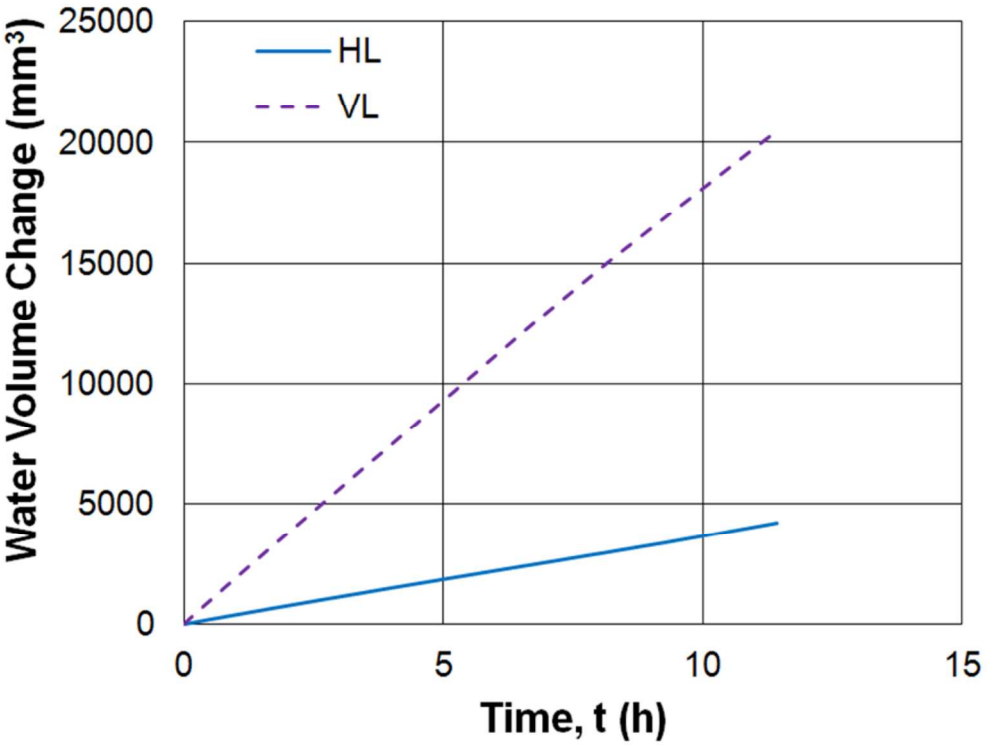

Figure 13. Typical water volume change curve during permeability measurement of applied matric suction up to 75 kPa

381x285mm (96 x 96 DPI)

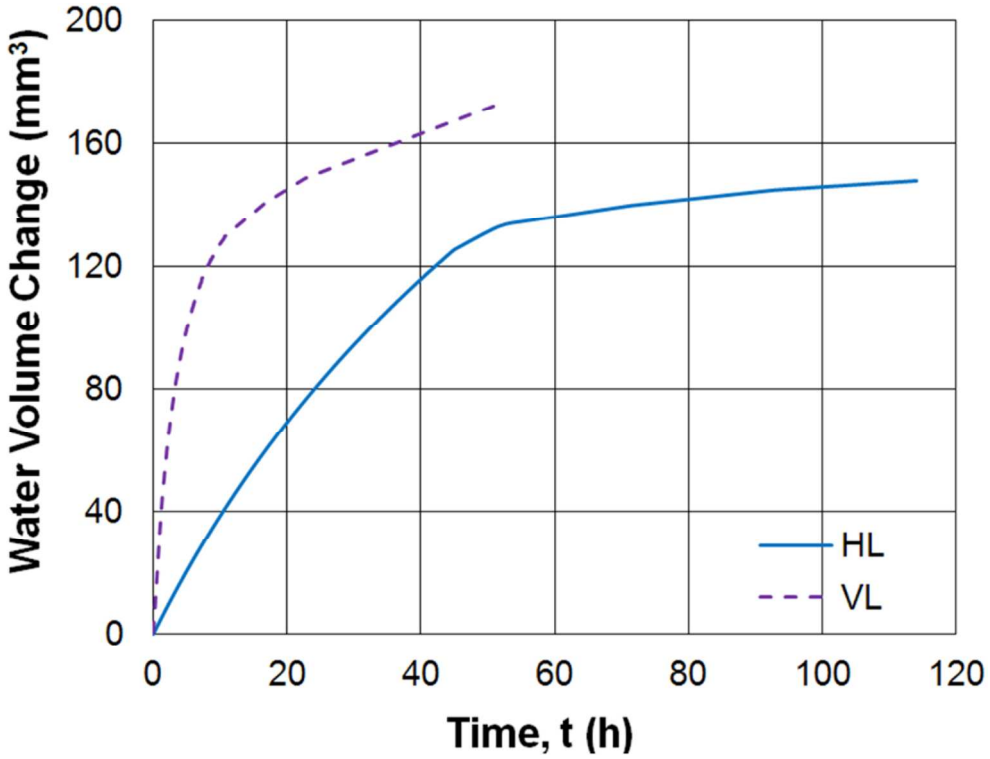

Figure 14. Typical water volume change curve during permeability measurement of applied matric suction of 90 kPa onwards

381x285mm (96 x 96 DPI)

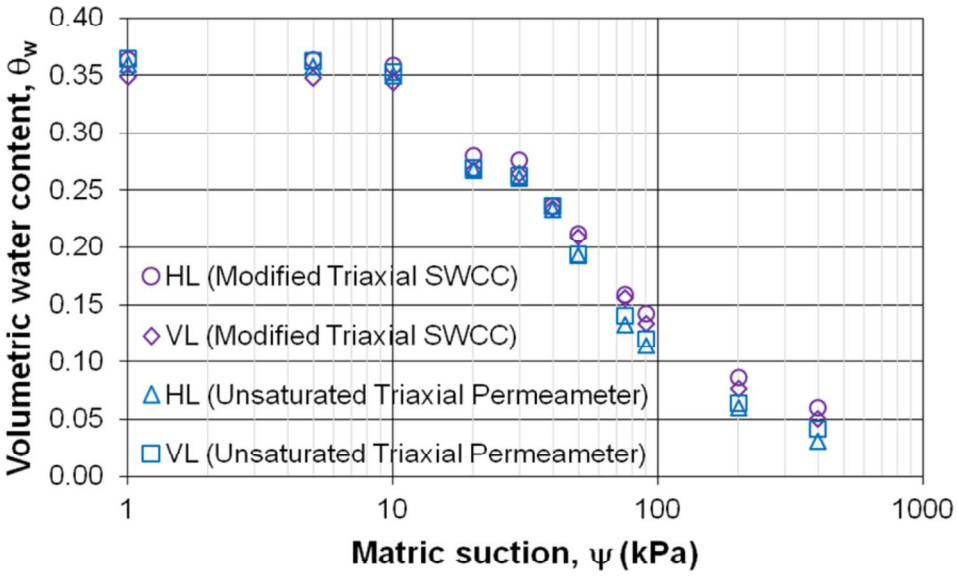

Figure 15. Drying SWCCs of Specimen A

381x285mm (96 x 96 DPI)

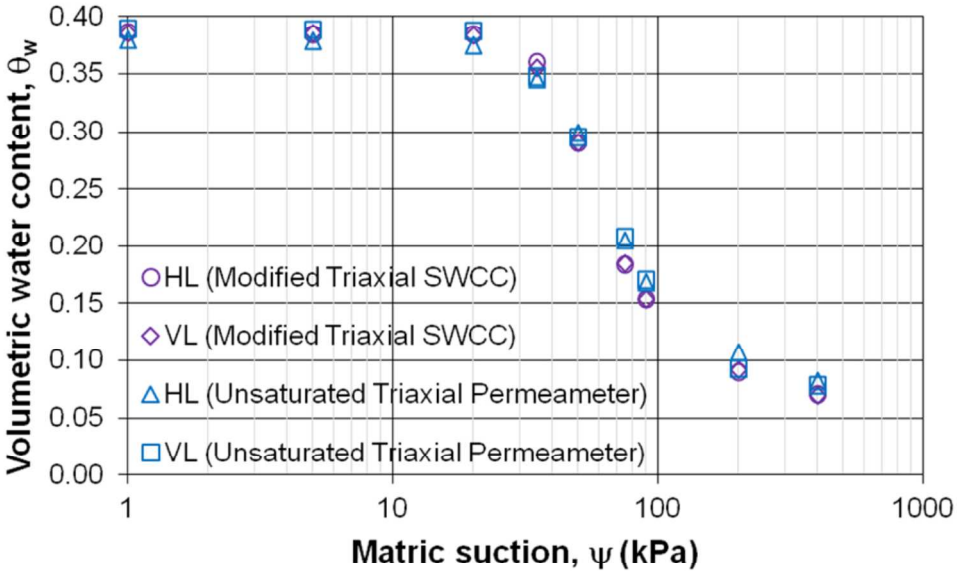

Figure 16. Drying SWCCs of Specimen B

381x285mm (96 x 96 DPI)

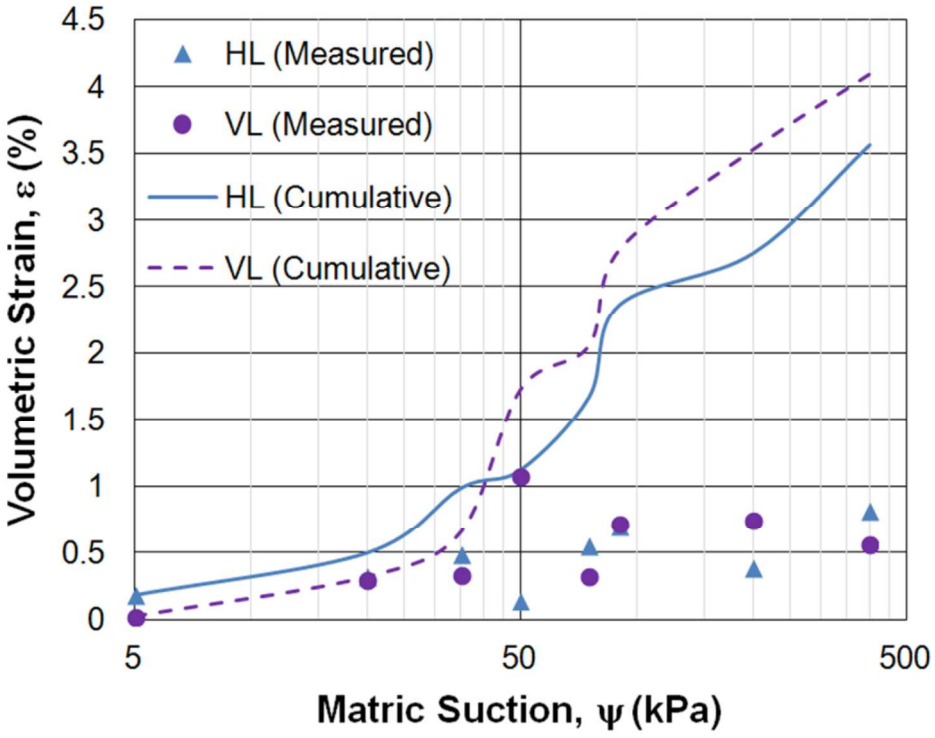

Figure 17. Typical volumetric strain measured during unsaturated permeability and SWCC tests

381x285mm (96 x 96 DPI)